Available online at www.sciencedirect.com
ScienceDirect
Journal of the Mechanics and Physics of Solids 56 (2008) 200–214
JOURNAL OF THE MECHANICS AND PHYSICS OF SOLIDS
www.elsevier.com/locate/jmps

On a new extended finite element method for dislocations: Core enrichment and nonlinear formulation ☆

Robert Gracie, Jay Oswald, Ted Belytschko*,[1]

Department of Mechanical Engineering, Northwestern University, 2145 Sheridan Road, Evanston, IL 60208-3111, USA

Received 13 November 2006; received in revised form 11 June 2007; accepted 1 July 2007

Abstract

A recently developed finite element method for the modeling of dislocations is improved by adding enrichments in the neighborhood of the dislocation core. In this method, the dislocation is modeled by a line or surface of discontinuity in two or three dimensions. The method is applicable to nonlinear and anisotropic materials, large deformations, and complicated geometries. Two separate enrichments are considered: a discontinuous jump enrichment and a singular enrichment based on the closed-form, infinite-domain solutions for the dislocation core. Several examples are presented for dislocations constrained in layered materials in 2D and 3D to illustrate the applicability of the method to interface problems.

Keywords: Dislocations; Interfaces; Extended finite element method; Peach–Koehler force; Nonlinear

1. Introduction

A new finite element method (FEM) for modeling dislocations has been described in Gracie et al. (2007) and Belytschko and Gracie (2007). In this method, dislocations are modeled by lines or surfaces of discontinuity, where one surface of the discontinuity is displaced relative to the other by the Burgers vector, as in the dislocation model of Volterra (1907), who conceptualized a dislocation as a cut, followed by a displacement and then a reattachment of the material of the two sides of the cut.

The method has a high degree of generality and it is straight-forward to apply it to problems with grain boundaries and material interfaces, and to anisotropic and nonlinear materials. The method can easily be incorporated into existing finite element software since the effect of the interior discontinuities that model the dislocations appear in the discrete equations only as external forces.

The methodology described here falls in the class of extended (generalized) finite element methods (XFEM), where local features of the solution are added to the standard finite element approximation. This concept was

☆This paper is in honour of the achievements of Alan Needleman and Viggo Tvergaard on the belated celebration of their 60th birthdays.

*Corresponding author.
E-mail address: tedbelytschko@northwestern.edu (T. Belytschko).
[1]Walter P. Murphy and McCormick Professor of Mechanical Engineering.

0022-5096/$ - see front matter © 2007 Elsevier Ltd. All rights reserved.
doi:10.1016/j.jmps.2007.07.010

introduced for discontinuous fields in Belytschko and Black (1999) and Moës et al. (1999); the tangential enrichment adopted here was introduced in Belytschko et al. (2001) for modeling shear bands. We use the methodology with level sets, as introduced in Stolarska et al. (2001) and Belytschko et al. (2001). To reinitialize the level sets, a fast marching method is employed as described by Chopp (2001).

Recent work with the method has shown that modeling the core of a dislocation by simple discontinuous models such as in Gracie et al. (2007) does not yield an optimal numerical method. The difficulty is that the Peach–Koehler force can then only be computed by a J-integral. Since the J-integral requires a patch with a radius of at least three elements, this requires very fine meshes to resolve the stress fields generated by dislocation interactions.

In this paper, we introduce a method where the dislocation is modeled by a discontinuity away from the core but an enrichment is employed around the core. This enrichment is based on closed-form solutions for dislocations that can be quite different than the problem at hand. For example, the infinite domain screw dislocation can be used in problems with interfaces and complex finite geometry. Adding this enrichment entails no additional complications and with some new developments described here, is as fast as the previous method. With this method, the Peach–Koehler force can be directly computed from the finite element stress field with a high degree of accuracy.

We also develop the equations for dislocations in media with nonlinear material properties and large deformations. These equations are given for the fully nonlinear case. In problems where the deformation is small, the effect of the dislocation appears only in the right-hand side of the linearized equations. This is an attractive attribute as it allows the method to be easily incorporated into standard finite elements, and for the case of dislocation dynamics (DD) simulations, the stiffness matrix need only be assembled and factored at the initial time step.

The majority of current DD methods are based on the superposition of infinite domain dislocation solutions, (Amodeo and Ghoniem, 1990; Kubin and Canova, 1992; Hirth et al., 1996; Schwarz and Tersoff, 1996). In two dimensions, these solutions are known analytically for isotropic materials; however, in three dimensions they take the form of integral equations. In general, isotropic material models are used in the above methods, though this assumption is known to introduce errors of 20–30% for crystal lattices (Hirth and Lothe, 1982). Even in single material systems, the solution of infinite domain integral equations for anisotropic materials can be very computationally demanding. Furthermore, multi-material Green's functions are available for only a few geometries; a recent one for layer materials was given by Han and Ghoniem (2005).

An alternative class of methods are those where the image field is computed. One of the most popular is the method of van der Giessen and Needleman (1995), where the image field is computed by the FEM. The solution on a finite domain is obtained by applying the image tractions from infinite domain solutions of all dislocations to the boundary of the model. The Peach–Koehler force at each dislocation is obtained by summing the contributions of all other dislocations. This superposition character of this method is one of its weaknesses when applied to large problems. On the other hand, the image field which is computed in the method is quite smooth, so the resolution requirements are modest. Other image-field methods are those of Schwarz (1999) and Fivel et al. (1996).

Recently, several dislocation methods have been developed that are related to our method (Wang et al., 2001a; Lemarchand et al., 2001; Ventura et al., 2005; Denoual, 2004; Roy and Acharya, 2005). These methods are not based on superposition of infinite domain fields; instead the equilibrium fields are determined directly, often by FEM. In the discrete-continuum model (DCM) of Lemarchand et al. (2001) the dislocations are treated as plastic strains. This model has been used to study a threading dislocation in an anisotropic thin film (Groh et al., 2003). Acharya (2001) and Roy and Acharya (2005) have developed a field theory DD model. Most of the above methods have only been applied to relatively simple problems. An exception is the phase field method (PFM) of Wang et al. (2001a,b) where dislocation multiplication was modeled in three dimensions. The PFM is similar to our method, but the dislocation is smeared (i.e. regularized) and a rather coarse model of the core is employed. The elastic strain energy contribution in the evolution equation is computed by a fast Fourier transform (FFT). In the Denoual (2004, 2007) the FFT calculations are replaced by FEM simulations, leading to a more flexible method.

An outline of the paper is as follows. Section 2 describes the basic concept of our method. In Section 3, we present the discrete FEM equations for linear and nonlinear models. The computation of the Peach–Koehler

force is presented in Section 4. In Section 5, several examples are considered. In the first, the convergence of the error in the Peach–Koehler force is studied for a single edge dislocation interacting with a bimaterial interface. We also compare the XFEM solution with analytical expressions for stresses in a dislocation loop. In a third problem we study a dislocation loop constrained in a thin Cu film between two Ni layers.

2. XFEM approximation

We denote the reference domain of the body by Ω_0 and its boundary by Γ_0. The boundary consists of a prescribed displacement boundary Γ_{0u} on which displacements $\bar{\mathbf{u}}$ are given and prescribed traction boundary Γ_{0t} where tractions $\bar{\mathbf{t}}_0$ are given. The image of Ω_0 in its current configuration is denoted by Ω and the images of the other entities are denoted by the same symbols with the subscript "naught" omitted, as shown in Fig. 1. We will distinguish tensors and matrices from scalars by boldface; we will also use Einstein notation with repeated indices denoting sums and commas denoting partial derivatives.

The n_{D} dislocations are modeled as discontinuities in the displacements on surfaces Γ^{α}_{0d}, $\alpha = 1 \ldots n_{\mathrm{D}}$. For convenience we denote the union of all discontinuities by Γ_{0d} where $\Gamma_{0d} = \bigcup_{\alpha} \Gamma^{\alpha}_{0d}$. We denote the spacial coordinates by $\mathbf{x}$, the material coordinates by $\mathbf{X}$. The motion is described by

$$\mathbf{x} = \boldsymbol{\phi}(\mathbf{X}, t) \tag{1}$$

and the displacement is given by

$$\mathbf{u} = \mathbf{x} - \mathbf{X}. \tag{2}$$

The displacement field at material point $\mathbf{X}$ and at time t is additively decomposed into two parts

$$\mathbf{u}(\mathbf{X}, t) = \mathbf{u}^{\mathrm{C}}(\mathbf{X}, t) + \mathbf{u}^{\mathrm{D}}(\mathbf{X}, t), \tag{3}$$

where $\mathbf{u}^{\mathrm{C}}(\mathbf{X}, t)$ is the standard continuous part of the displacement field and $\mathbf{u}^{\mathrm{D}}(\mathbf{X}, t)$ is the discontinuous or enriched part. The continuous part is given by the standard finite element approximation

$$\mathbf{u}^{\mathrm{C}}(\mathbf{X}, t) = \sum_{I \in S} N_I(\mathbf{X}) \mathbf{u}_I(t), \tag{4}$$

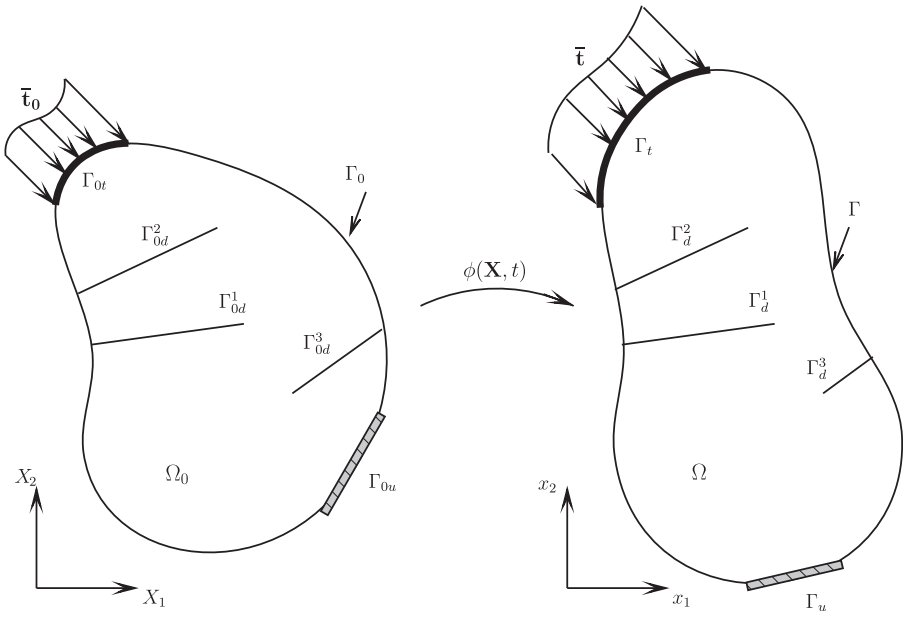

Fig. 1. Notation convention for the reference and current domain of a body with dislocations Γ^{α}_d.

where $\mathbf{u}_I^{\mathrm{T}} = \{u_{xI}, u_{yI}, u_{zI}\}$ are the nodal displacements, $N_I(\mathbf{X})$ are the shape functions and S is the set of all nodes, and

$$\mathbf{u}^{\mathrm{D}}(\mathbf{X}, t) = \sum_{\alpha=1}^{n_{\mathrm{D}}} \boldsymbol{\Psi}^{\alpha}(\mathbf{X}, t). \tag{5}$$

The function $\boldsymbol{\Psi}^{\alpha}(\mathbf{X}, t)$ is often called an enrichment function since it enriches the standard approximation with what is locally known about the solution.

Two enrichment functions $\boldsymbol{\Psi}^{\alpha}(\mathbf{X}, t)$ are used in our method. The first adds a discontinuity on a closed-surface in the domain; e.g. an edge dislocation enrichment introduces a tangential jump of constant magnitude across the slip plane. This enrichment can be modified in the vicinity of the core to produce slip profiles consistent with Peierls–Nabarro models. The second enrichment adds a field defined by analytical functions characteristic of core mechanics in the vicinity of the core.

To define the discontinuous part of the displacement approximation, (5), we use level set functions as in Belytschko et al. (2001), Stolarska et al. (2001), and Gravouil et al. (2002); level sets have been used to model dislocations by Xiang et al. (2003, 2004), but by a different method. We define the surface of the glide plane of dislocation α at time t by $f^{\alpha}(\mathbf{X}, t) = 0$ and $g^{\alpha}(\mathbf{X}, t) > 0$; the core of the dislocation is then given by the intersection of the surface $f^{\alpha}(\mathbf{X}, t) = 0$ and the surface $g^{\alpha}(\mathbf{X}, t) = 0$, see Fig. 2.

In the XFEM method, undesirable errors occur at the edge of the core enrichment; this has previously been noted by Chessa et al. (2003) in another XFEM application. These are particularly troublesome in DD methods because they affect the Peach–Koehler forces. To circumvent these difficulties we use a discontinuous Galerkin formulation at the edge of the core-enriched subdomain.

2.1. Discontinuous enrichment

In the following we describe the enrichment functions used in Eqs. (3) and (5) to model the dislocations. Two enrichment functions are used: a discontinuous enrichment, as in Gracie et al. (2007), which is always employed to model the discontinuity across the glide plane far from the core, and a core enrichment which is added in the vicinity of the core.

Let $\mathscr{S}^{\alpha}$ be the set of nodes belonging to the elements in $\mathscr{E}^{\alpha}$ where $\mathscr{E}^{\alpha}$ is the set of all elements with at least one edge crossed by the glide plane of dislocation α. The enrichment functions $\Psi^{\alpha}(\mathbf{X}, t)$ for the discontinuous (or jump) enrichment are

$$\boldsymbol{\Psi}_H^{\alpha}(\mathbf{X}, t) = \mathbf{b}^{\alpha} \sum_{J \in \mathscr{S}^{\alpha}} N_J(\mathbf{X})(H(f^{\alpha}(\mathbf{X}, t)) - H_J^{\alpha}) H(g^{\alpha}(\mathbf{X}, t)). \tag{6}$$

In the above $H(\bullet)$ is the standard Heaviside step function, $H_J^{\alpha} = H(f^{\alpha}(\mathbf{X}_J, t))$, $\mathbf{b}^{\alpha}$ is the Burgers vector, and N_J are the enrichment shape functions.

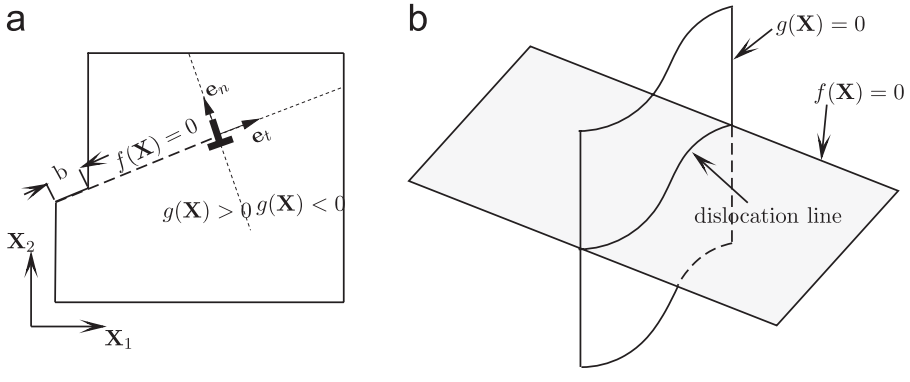

Fig. 2. (a) Definition of an edge dislocation by level sets $f(\mathbf{X})$ and $g(\mathbf{X})$; (b) definition of a dislocation loop by level sets $f(\mathbf{X})$ and $g(\mathbf{X})$.

The enrichment function for dislocation α vanishes outside of the domain formed by the union of the elements in $\mathscr{E}^{\alpha}$. So the jump enrichment for a particular dislocation is included only in a small part of the finite element model. The jump enrichment function vanishes at all nodes, i.e. $\mathbf{\Psi}^{\alpha}_{H}(\mathbf{X}_I) = 0, \forall I \in \mathscr{S}^{\alpha}$ so essential boundary conditions can be applied directly to the standard nodal degrees of freedom as in the standard FEM.

2.2. Singular core enrichment

Let Ω_α be a circular domain of radius r_α with boundary $\partial\Omega_\alpha$ centered at dislocation core α, as shown in Fig. 3(a). Let $\mathscr{S}^{\infty}_{\alpha}$ be the set of all nodes in Ω_α and $\mathscr{S}^{H}_{\alpha}$ be the set of all nodes of elements cut by glide plane α not in $\mathscr{S}^{\infty}_{\alpha}$. The nodes in sets $\mathscr{S}^{\infty}_{\alpha}$ and $\mathscr{S}^{H}_{\alpha}$ are illustrated in Fig. 3(b) for a single dislocation. Nodes in set $\mathscr{S}^{\infty}_{\alpha}$ are enriched with the singular core enrichment, while nodes in $\mathscr{S}^{H}_{\alpha}$ are enriched with the jump enrichment described (6) in the previous section.

The local singular core enrichment depends on the type of dislocation, but in all cases are derived from general solutions to infinite domain problems. For the edge component of a dislocation the enrichment is

$$\mathbf{\Psi}^{\alpha}_{\mathrm{C}} = \frac{\mathbf{b}^{\alpha}\cdot\mathbf{e}_t}{2\pi}\begin{pmatrix} \left(\tan^{-1}\left(\dfrac{y'}{x'}\right) + \dfrac{x'y'}{2(1-\nu)(x'^2+y'^2)}\right)\mathbf{e}_t \\ -\left(\dfrac{1-2\nu}{4(1-\nu)}\ln(x'^2+y'^2) + \dfrac{x'^2-y'^2}{4(1-\nu)(x'^2+y'^2)}\right)\mathbf{e}_n \end{pmatrix}. \tag{7}$$

For the screw component the enrichment is

$$\mathbf{\Psi}^{\alpha}_{\mathrm{C}} = \frac{\mathbf{b}^{\alpha}\cdot(\mathbf{e}_t\times\mathbf{e}_n)}{2\pi}\tan^{-1}\left(\frac{y'}{x'}\right)(\mathbf{e}_t\times\mathbf{e}_n), \tag{8}$$

where $x' = (\mathbf{X}-\mathbf{X}^{\alpha}_{\mathrm{c}})\cdot\mathbf{e}_t$, $y' = (\mathbf{X}-\mathbf{X}^{\alpha}_{\mathrm{c}})\cdot\mathbf{e}_n$ (see Fig. 2a), thus the enrichments are not problem specific. In the above, the unit vectors are expressed in terms of the level set functions that describe the configuration of the dislocation by $\mathbf{e}_t = -\vec{\nabla}g(\mathbf{X})$ and $\mathbf{e}_n = \vec{\nabla}f(\mathbf{X})$. In two dimensions, the basis vectors of the dislocation are prescribed by the problem. The complete enrichment for a dislocation with a core at $\mathbf{X}_{\mathrm{c}}$ is the sum of (6) and the edge and screw components given in Eqs. (7) and (8).

The core enrichment considered here is slightly different from that considered in Ventura et al. (2005). Here we have introduced the jump enrichment for the nodes of elements cut by the glide plane that are sufficiently far from the dislocation core. Since the strain gradients are small far from the core, the adoption of the tangential enrichment away from the core reduces the computational cost of the singular core enrichment. Here we would like to remark that:

(1) The infinite domain solution is applicable for dislocations interacting with material interfaces, i.e. Ω^{α} is allowed to span material interfaces. This is because the FEM solution will supply the necessary image field which when added to the enrichment produces the correct solution.

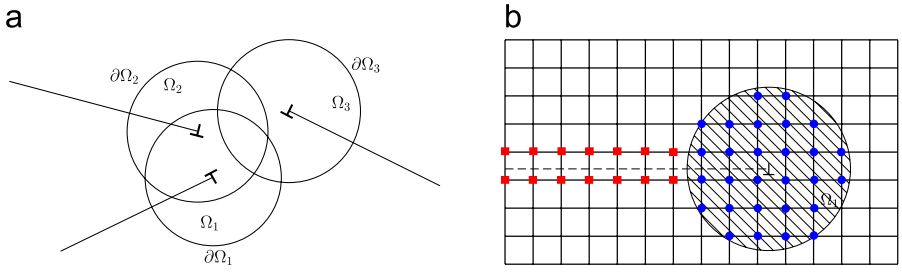

Fig. 3. (a) Illustration of the local domains Ω_α with boundaries $\partial\Omega_\alpha$ surrounding each dislocation core; (b) definition of the sets $\mathscr{S}^{\infty}_{\alpha}$ and $\mathscr{S}^{H}_{\alpha}$. The nodes in $\mathscr{S}^{\infty}_{\alpha}$ are represented by blue circles and the nodes in $\mathscr{S}^{H}_{\alpha}$ are represented by red squares.

(2) Non-singular dislocations can be modeled by using the non-singular dislocation solutions derived by Cai et al. (2006).
(3) The accuracy of the singular core enrichment may be improved by increasing the size of the enrichment domains Ω^{α}.

3. Governing equations

We next derive the finite element equations for a dislocation model applicable to nonlinear hyperelastic materials and large deformations. The nonlinear models of dislocations should become of importance as problems with large deformations and large rotations become of interest. A significant advantage of this method is that it can easily be applied to nonlinear problems. After developing the fully nonlinear equations, we specialize the equations to linear elastic materials.

The discrete equations are obtained by the theorem of minimum potential energy, which states that the solution $\mathbf{u}(\mathbf{X})$ is a stationary point of

$$\Pi = \int_{\Omega_0/\Gamma_{0d}} W(\mathbf{F}(\mathbf{u}))\,\mathrm{d}\Omega_0 - \int_{\Omega_0} \mathbf{u}\cdot\mathbf{b}_0\,\mathrm{d}\Omega_0 - \int_{\Gamma_{0t}} \mathbf{u}\cdot\bar{\mathbf{t}}_0\,\mathrm{d}\Gamma_0 \tag{9}$$

among all kinematically admissible displacements $\mathbf{u}$, where $W(\mathbf{F}(\mathbf{u}))$ is the stored potential energy in terms of the deformation gradient $\mathbf{F} = \partial\boldsymbol{\phi}/\partial\mathbf{X}$, $\mathbf{b}_0$ is the body force, and $\bar{\mathbf{t}}_0$ are the prescribed tractions. Note that the internal energy in Eq. (9) excludes the dislocation surfaces.

If we substitute Eqs. (3)–(5) into Eq. (9), take the derivative with respect to u_{iI} and set it equal to zero to determine the stationary points, we obtain

$$0 = \frac{\partial\Pi}{\partial u_{iI}} = \int_{\Omega_0/\Gamma_{0d}} \frac{\partial W}{\partial F_{ij}}\frac{\partial N_I}{\partial X_j}\,\mathrm{d}\Omega_0 - f_{iI}^{\mathrm{ext}}, \tag{10}$$

where

$$f_{iI}^{\mathrm{ext}} = \int_{\Omega_0} N_I b_{0i}\Omega_0 - \int_{\Gamma_{0t}} N_I \bar{t}_{0i}\,\mathrm{d}\Gamma_0. \tag{11}$$

We note that the first Piola–Kirchhoff stress is given by

$$P_{ij} = \frac{\partial W}{\partial F_{ij}} \tag{12}$$

so we can write the first term in Eq. (10) as

$$f_{iI}^{\mathrm{int}} = \int_{\Omega_0/\Gamma_{0d}} \frac{\partial N_I}{\partial X_j} P_{ij}(\mathbf{F}(\mathbf{u}^{\mathrm{C}} + \mathbf{u}^{\mathrm{D}}))\,\mathrm{d}\Omega_0. \tag{13}$$

Thus the discrete equations of equilibrium are the standard equations (see e.g. Belytschko et al., 2000)

$$f_{iI}^{\mathrm{int}} - f_{iI}^{\mathrm{ext}} = 0, \tag{14}$$

where the effect of the dislocations enters in the computation of the internal forces through the dependence of $\mathbf{P}$ on $\mathbf{u}^{\mathrm{D}}$ in Eq. (13).

In the small deformation linear case, a segregation of the effects of the dislocation, so that they appear entirely on the right-hand side of the linear equations, is possible. The above large displacement nonlinear formulation can be reduced to the linear case by replacing $\mathbf{P}$ with the Cauchy stress $\boldsymbol{\sigma}$, and restricting the constitutive equations to the linear elastic law.

$$\boldsymbol{\sigma}(\mathbf{u}) = \mathbf{C}\boldsymbol{\varepsilon}(\mathbf{u}), \tag{15}$$

where

$$\boldsymbol{\varepsilon}(\mathbf{u}) = \nabla_{\mathrm{sym}}\mathbf{u}. \tag{16}$$

The reference and current configurations do not need to be distinguished in the linear case, so we drop the subscripts "naught". Similarly, $\mathbf{x}$ and $\mathbf{X}$ need not be distinguished, so we use $\mathbf{x}$.

Then Eq. (13) becomes

$$f_{iI}^{\text{int}} = \int_{\Omega/\Gamma_d} \frac{\partial N_I}{\partial x_j} \sigma_{ij}(\boldsymbol{\varepsilon}(\mathbf{u}^{\text{C}} + \mathbf{u}^{\text{D}}))\, \mathrm{d}\Omega. \tag{17}$$

Invoking the strain displacement equation (16) and the finite element approximation (4), (5) and (6) gives

$$f_I^{\text{int}} = \int_{\Omega/\Gamma_d} \mathbf{B}^{\text{T}} \boldsymbol{\sigma}\,(\boldsymbol{\varepsilon}(\mathbf{u}^{\text{C}} + \mathbf{u}^{\text{D}}))\, \mathrm{d}\Omega = \int_{\Omega/\Gamma_d} \mathbf{B}^{\text{T}} \mathbf{C}(\mathbf{B}\mathbf{d} + \sum_{\alpha} \mathbf{D}^{\alpha} b^{\alpha})\, \mathrm{d}\Omega, \tag{18}$$

where for a 2D mesh of nn nodes $\mathbf{d}^{\text{T}} = \{\mathbf{u}_1, \mathbf{u}_2, \ldots, \mathbf{u}_{nn}\}^{\text{T}}$ and

$$\mathbf{B}_I = \begin{bmatrix} N_{I,x} & 0 \\ 0 & N_{I,y} \\ N_{I,y} & N_{I,x} \end{bmatrix}, \tag{19}$$

$$\mathbf{D}(\boldsymbol{\Psi}^{\alpha}) = \begin{bmatrix} \mathbf{e}_x \cdot \boldsymbol{\Psi}^{\alpha}_{,x} \\ \mathbf{e}_y \cdot \boldsymbol{\Psi}^{\alpha}_{,y} \\ \mathbf{e}_x \cdot \boldsymbol{\Psi}^{\alpha}_{,y} + \mathbf{e}_y \cdot \boldsymbol{\Psi}^{\alpha}_{,x} \end{bmatrix}. \tag{20}$$

The linear equations are then

$$\sum_{J \in S} \mathbf{K}_{IJ} \mathbf{u}_J + \sum_{\alpha=1}^{n_{\text{D}}} \mathbf{f}_I^{\text{D}\alpha} - \mathbf{f}_I^{\text{ext}} = 0, \tag{21}$$

where $\mathbf{f}^{\text{ext}}$ is given by Eq. (11) and $\mathbf{K}_{IJ}$ is the standard linear stiffness given by

$$\mathbf{K}_{IJ} = \frac{\partial \mathbf{f}_I^{\text{int}}}{\partial \mathbf{u}_J} = \int_{\Omega/\Gamma_d} \mathbf{B}_I^{\text{T}} \mathbf{C} \mathbf{B}_J\, \mathrm{d}\Omega. \tag{22}$$

The term $\mathbf{f}_I^{\text{D}\alpha}$ represents the effect of dislocation α, and is given by

$$\mathbf{f}_I^{\text{D}\alpha} = \frac{\partial \mathbf{f}_I^{\text{int}}}{\partial b^{\alpha}} b^{\alpha} = \int_{\Omega/\Gamma_d} \mathbf{B}_I^{\text{T}} \mathbf{C} \mathbf{D}^{\alpha} b^{\alpha}\, \mathrm{d}\Omega = \int_{\Omega/\Gamma_d} \mathbf{B}_I^{\text{T}} \boldsymbol{\sigma}(\mathbf{u}^{\text{D}})\, \mathrm{d}\Omega \quad \text{for } I \in \mathscr{S}^{\alpha}. \tag{23}$$

It can be seen from Eq. (21) that the finite element stiffness matrix for this method is identical to the standard linear stiffness and that the effect of the dislocations enter the equations entirely through the forces $\mathbf{f}_I^{\text{D}\alpha}$ given by Eq. (23).

For the tangential jump enrichment, the force due to the dislocations (23) is given by

$$\mathbf{f}_I^{\text{D}\alpha} = \begin{cases} \int_{\Omega} \mathbf{B}_I^{\text{T}} \mathbf{C} \mathbf{D}^{\alpha}(\boldsymbol{\Psi}^{\alpha}_H) b^{\alpha}\, \mathrm{d}\Omega & \text{for } I \in \mathscr{S}^{\alpha}_H, \\ 0 & \text{otherwise.} \end{cases} \tag{24}$$

The force due to the dislocations (23) for the local singular core enrichment is given by

$$\mathbf{f}_I^{\text{D}\alpha} = \begin{cases} \int_{\Omega} \mathbf{B}_I^{\text{T}} \mathbf{C} \mathbf{D}(\boldsymbol{\Psi}^{\alpha}_{\text{C}})\, \mathrm{d}\Omega & \text{for } I \in \mathscr{S}^{\alpha}_{\infty}, \\ \int_{\Omega} \mathbf{B}_I^{\text{T}} \mathbf{C} \mathbf{D}^{\alpha}(\boldsymbol{\Psi}^{\alpha}_H) b^{\alpha}\, \mathrm{d}\Omega & \text{for } I \in \mathscr{S}^{\alpha}_H, \\ 0 & \text{else} \end{cases} \tag{25}$$

and $\mathbf{D}(\boldsymbol{\Psi}^{\alpha})$ is given by Eq. (20).

In the element containing dislocation core α, the integrand in Eq. (25) is singular and therefore numerical integration is expensive. To reduce the computational cost, we recast the domain integral in Eq. (25a) into

an equivalent contour integral as suggested in Ventura et al. (2005). Applying Gauss's theorem we obtain

$$\mathbf{f}_I^{\mathrm{D}\alpha} = \int_{\partial\Omega^\alpha} \mathbf{N}_I \boldsymbol{\sigma}^\infty(\mathbf{x}, \mathbf{x}_\mathrm{c}^\alpha) \cdot \mathbf{n}^\alpha \, \mathrm{d}\Gamma - \int_{\Omega^\alpha} \mathbf{B}_I^{\mathrm{T}} \, \mathrm{div}(\boldsymbol{\sigma}^\infty(\mathbf{x}, \mathbf{x}_\mathrm{c}^\alpha)) \, \mathrm{d}\Omega \quad \text{for } I \in S_\infty^\alpha, \tag{26}$$

where $\boldsymbol{\sigma}^\infty$ is the stress corresponding to $\mathbf{u}^{\mathrm{D}}$ in Eqs. (7) and (8).

By equilibrium $\mathrm{div}(\boldsymbol{\sigma}^\infty(\mathbf{x}, \mathbf{x}_\mathrm{c}^\alpha)) = 0$, so Eq. (26) can be simplified to

$$\mathbf{f}_I^{\mathrm{D}\alpha} = \int_{\partial\Omega^\alpha} \mathbf{N}_I \boldsymbol{\sigma}^\infty(\mathbf{x}, \mathbf{x}_\mathrm{c}^\alpha) \cdot \mathbf{n}^\alpha \, \mathrm{d}\Gamma \quad \text{for } I \in S_\infty^\alpha \tag{27}$$

where $\mathbf{n}^\alpha$ is the outward unit normal to domain Ω^α, see Fig. 3, so that the evaluation of the dislocation forces is reduced to a contour integral.

4. Peach–Koehler force and dislocation motion

The Peach–Koehler force provides the driving force for dislocation motion. Peach and Koehler (1950) derived the force $\mathbf{F}^\alpha$ acting on dislocation α per unit length δs of a dislocation line as

$$\frac{\delta \mathbf{F}^\alpha}{\delta s} = -\boldsymbol{\xi}^\alpha \times (\tilde{\boldsymbol{\sigma}} \cdot \mathbf{b}^\alpha), \tag{28}$$

where $\boldsymbol{\xi}$ is a unit vector along the dislocation line s, $\tilde{\boldsymbol{\sigma}}$ is the stress from all sources except the self-stress of dislocation α and $\mathbf{b}^\alpha$ is its Burgers vector.

We have used two methods to compute the Peach–Koehler force: (1) J-integrals and (2) direct computation of Eq. (28) with $\tilde{\boldsymbol{\sigma}}$ computed from the FEM solution. In the J-integral approach (Eshelby, 1951), the Eshelby tensor is integrated over a closed contour about the dislocation core. The domain form of the J-integral of Moran and Shih (1987) was adopted due to its improved accuracy.

The primary limitation of the contour integral approach is that the integral must be taken over a domain that does not contain any other dislocation cores. It was found in Belytschko and Gracie (2007) that for cylindrical domains, a minimum internal radius of $3h_\mathrm{e}$, where h_e is the average element size in the vicinity of the dislocation core, was required for accurate results. So to obtain accurate Peach–Koehler forces, the mesh size must be smaller than one third of the distance separating two dislocation cores.

When the singular core enrichment is used, the stress $\tilde{\boldsymbol{\sigma}}$ in Eq. (28) is given by

$$\tilde{\boldsymbol{\sigma}}(\mathbf{x}_\mathrm{c}^\alpha) = \boldsymbol{\sigma}^{\mathrm{C}}(\mathbf{x}_\mathrm{c}^\alpha) + \sum_{\beta \in \mathscr{S}^{\beta/\alpha}} \boldsymbol{\sigma}^\infty(\mathbf{x}_\mathrm{c}^\alpha, \mathbf{x}_\mathrm{c}^\beta), \tag{29}$$

where $\boldsymbol{\sigma}^{\mathrm{C}}(\mathbf{x}_\mathrm{c}^\alpha)$ is the stress from the standard part of the displacement approximation, Eq. (4) and $\mathscr{S}^{\beta/\alpha}$ is the set of all dislocations β with Ω^β containing $\mathbf{x}_\mathrm{c}^\alpha$ and $\beta \neq \alpha$; this is a counterpart of the equation derived in van der Giessen and Needleman (1995). For example, in Fig. 3(a), $\mathscr{S}^{\beta/1} = \{2\}$, $\mathscr{S}^{\beta/2} = \{1\}$, and $\mathscr{S}^{\beta/3} = \{\emptyset\}$. For clarity, the stress due to dislocations θ, $\theta \notin \mathscr{S}^{\beta/\alpha}$ and $\theta \neq \alpha$ is included in Eq. (29) through $\boldsymbol{\sigma}^{\mathrm{C}}$.

The evolution of the dislocation line is computed by the evolution of the level sets f and g, introduced in Section 2. The velocity of the dislocation line is projected throughout the level set domain and the level sets are advected by the method given in Chessa et al. (2002). The dislocation line velocity can be determined using standard relationships between velocity and the Peach–Koehler force, see for example Bulatov and Cai (2006).

5. Examples

5.1. Dislocation near a bimaterial interface

We consider a $1\,\mu\mathrm{m} \times 1\,\mu\mathrm{m}$ bimaterial domain with an edge dislocation near the interface. The material interface bisects the domain along the plane $x = 0.5\,\mu\mathrm{m}$, as shown in Fig. 4(a). For $x < 0.5\,\mu\mathrm{m}$ the material properties are $E = 94.7\,\mathrm{GPa}$ and $\nu = 0.276$, while for $x > 0.5\,\mu\mathrm{m}$ $E = 31\,\mathrm{GPa}$ and $\nu = 0.276$. A dislocation core is located at $\mathbf{x}_\mathrm{c} = (0.75\,\mu\mathrm{m}, 0.5\,\mu\mathrm{m})$ with Burgers vector $b = 0.25\,\mathrm{nm}$ in the x-direction, and with a horizontal glide plane extending to the left. The domain is discretized by a structured mesh of bilinear elements, and the

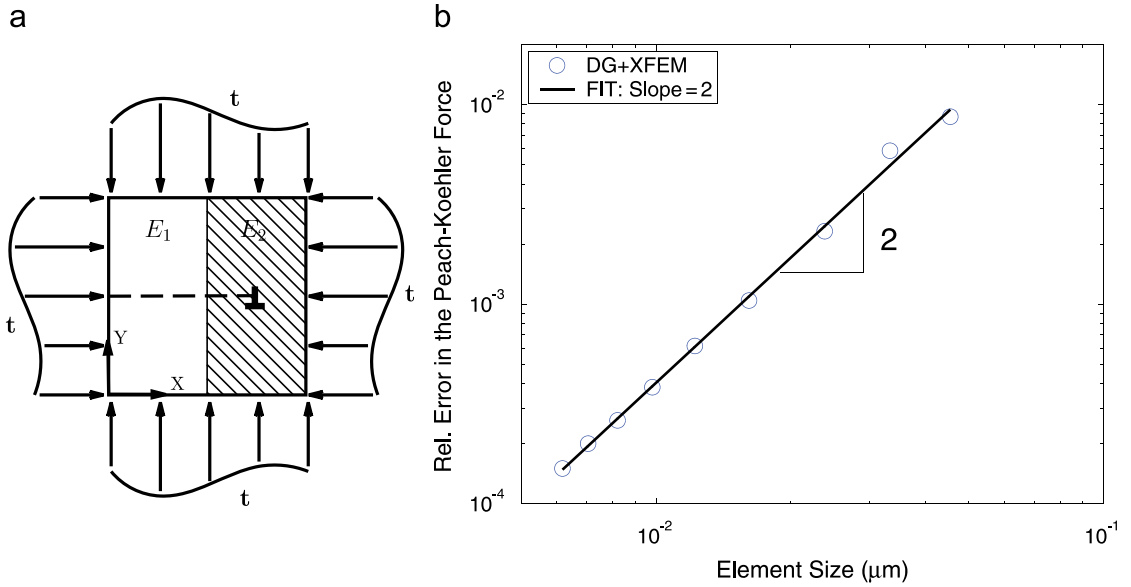

Fig. 4. (a) Nomenclature for an edge dislocation near a bimaterial interface between two semi-infinite domains; (b) convergence of the relative error of the glide component of the Peach–Koehler force.

singular core enrichment given in Eq. (7) is used over a circular domain of radius $r = 0.15\,\mu\text{m}$. On the boundaries of the model traction boundary conditions corresponding to the analytical solution of an edge dislocation near a bimaterial interface separating two semi-infinite domains are applied (Head, 1953; Dundurs and Sendeckyj, 1965). Rigid body motion is eliminated by fixing the displacement of the bottom left corner of the domain in both directions and by fixing the displacement of the bottom right corner in the y-direction.

The convergence of the relative error in the glide force on the dislocation core with decreasing element size is shown in Fig. 4b. A convergence rate of two is obtained, which is the optimal rate for the 4-node element employed here. Convergence is monotonic with the Peach–Koehler force underestimated for coarse meshes.

5.2. Circular dislocation loop

We next study a dislocation loop in three dimensions. Consider a circular dislocation loop in an $L \times L \times L$, $L = 120\,\text{nm}$, domain with material properties $E = 100\,\text{GPa}$ and $\nu = 0.34$, as shown in Fig. 6. The dislocation loop is centered at $(L/2, L/2, L/2)$ and has a radius $a = 30\,\text{nm}$. The dislocation lies on a plane with normal parallel to the z-axis and with a Burgers vector of magnitude $b = 0.25\,\text{nm}$ and direction parallel to the x-axis. We apply displacement boundary conditions corresponding to the solution of the dislocation in an infinite domain (Hirth and Lothe, 1982) and evaluate the accuracy of XFEM in recovering the solution inside the domain. The analytical solution requires the evaluation of three integrals which we numerically integrate using an adaptive Gauss quadrature procedure. We compare the XFEM result to the exact solution by plotting the stress components (Fig. 5), σ_{xx}, and σ_{xz} along a line given by $y = L/2$ and $z = L/2 + \varepsilon$, where $\varepsilon = 5b$. As seen from Fig. 5, the stress approximations from the discontinuous enrichment exhibit a noticeable amount of jaggedness but this is easily corrected by numerical smoothing (Fig. 6).

5.3. Dislocation motion in thin films

In small systems domain boundaries and material interfaces play a critical role in the stresses driving dislocation motion. In very thin films, dislocation sources cannot emit multiple dislocations and the Hall–Petch mechanism is not dominant. Instead dislocations will glide along the thin film, parallel to the material interfaces under the influence of an applied stress; this is illustrated in Fig. 7 as the transition from

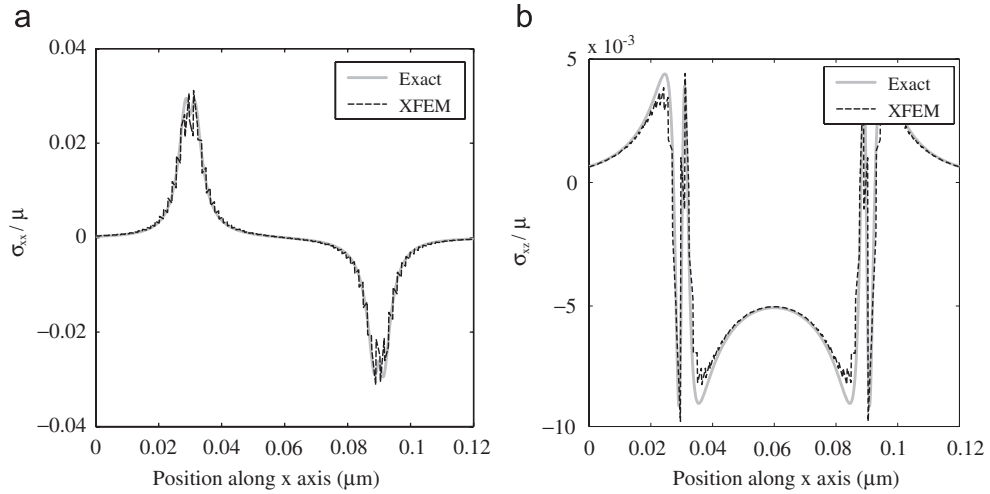

Fig. 5. Comparison of stress across a circular dislocation loop between the exact analytical solution, and the XFEM approximation with a finite element mesh of $90 \times 90 \times 90$ elements, (2 MDOF).

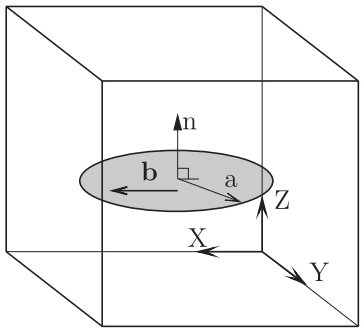

Fig. 6. Nomenclature for a circular dislocation in an infinite domain.

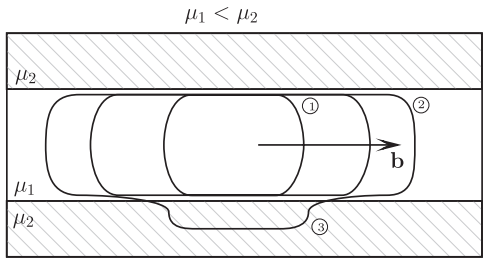

Fig. 7. Illustration of the dislocation motion along the (1 1 1) plane of a very thin FCC film between two stiffer material layers. Deformation from configuration 1 to 2 occurs by slip confined to the thin film, while the deformation from configuration 2 to 3 occurs by overcoming the Koehler barrier between the thin film and bottom stiff layer.

states 1 to 2. If the slip parallel to the material interfaces is impeded by obstacles such as other threading dislocations on intersecting slip planes, the applied stress can be sufficient to overcome the Koehler barrier of the interface, illustrated as the transition from states 2 to 3 in Fig. 7.

Most theoretical and numerical models for thin films are based on simplified treatments of the image stresses on the material interfaces. For example, in many superposition based dislocation methods, thin film boundaries are simply modeled as rigid interfaces (Schwarz and Tersoff, 1996; Blanckenhagen et al., 2003; van der Giessen and Needleman, 2003). The importance of accurately accounting for free surfaces has been illustrated in Han et al. (2006). The influence of material interfaces on dislocation motion has been treated by Ghoniem and Han (2005) and Groh et al. (2003). The former is limited to parallel material interfaces, whereas the accuracy of the latter is limited by mesh resolution.

5.3.1. *Slip across a material interface: the Koehler barrier*

Here we consider a 120 nm × 120 nm × 120 nm cubic domain as shown in Fig. 8(a) consisting of two parallel Ni layers ($\mu_2 = 94.5\,\text{GPa}$, $\nu_2 = 0.276$) of thickness $t_{\text{Ni}} = 40\,\text{nm}$ separated by a Cu layer ($\mu_1 = 31\,\text{GPa}$, $\nu_1 = 0.416$) of thickness $t_{\text{Cu}} = 40\,\text{nm}$. The Ni–Cu interfaces are perfectly coherent. The [1 0 0], [0 1 0] and [0 0 1] directions are coaxial with $\mathbf{e}_x$, $\mathbf{e}_y$ and $\mathbf{e}_z$, respectively. Slip in the Cu film will occur along the (1 1 1) plane with Burgers vector of magnitude $b = 0.256\,\text{nm}$ and direction $[\bar{1}\,1\,0]$. So the dislocation line nearest the material interface is of screw character while that in the middle of the film is of edge character. The bottom of the domain is fixed and the top of the domain is subjected to a state of biaxial stress.

We first study the applied stress required for the screw component of a dislocation loop in the Cu layer to overcome the Koehler barrier with a 2D model using the DG formulation with the singular core enrichment. In linear elasticity, a dislocation in a soft material will experience an infinite barrier when approaching a stiffer material (Dundurs and Sendeckyj, 1965). Dislocation motion across such a material interface can therefore only be modeled empirically in any linear elastic dislocation model. The applied stress required to overcome the Koehler barrier will be taken as that required to drive the dislocation to within a distance of $2b$ from either material interface (Koehler, 1970).

A 2D representation of the dislocation loop is a good first order approximation since the dislocation line near the material interfaces are known to be nearly parallel to the interface. Our 2D model consists of a screw dislocation dipole, with the slip plane at an angle of $\cos^{-1}\sqrt{\frac{2}{3}}$ from the X'-axis, as shown in Fig. 8(b) and (c). The mobility of the dislocations is isotropic with a magnitude of $10^4\,\text{Pa}^{-1}\,\text{s}^{-1}$. Fig. 9 shows the equilibrium distance between the upper screw dislocation and the upper Ni–Cu interface as a function of the applied stress. The Koehler barrier is overcome by an applied shear stress of about 425 MPa. This stress is smaller than that from the Koehler model (Koehler, 1970), which does not consider free surfaces. Such forces would tend to drive the dislocations towards the interfaces, decreasing the applied stress required to overcome the Koehler barrier. Therefore, it can be seen that rigorous consideration of the influence of material interfaces is crucial in modeling thin films.

The 2D model presented has some notable limitations. First, it does not consider partial dislocations. The applied stress required for partial dislocations to slip across material interfaces is known to be lower than that of perfect dislocations (Koehler, 1970; Rao and Hazzledine, 2000). Second, the model cannot account for the

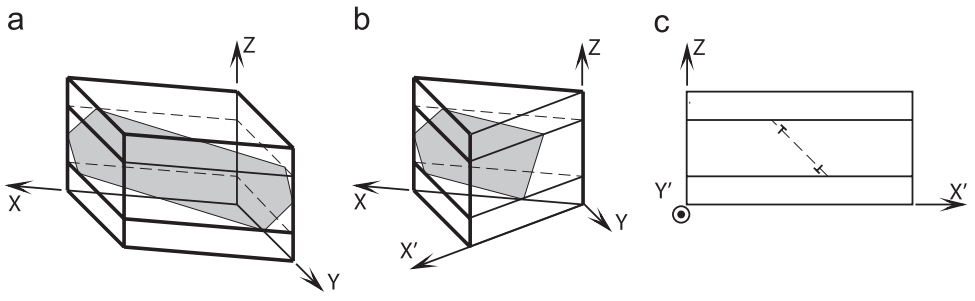

Fig. 8. Illustration of (1 1 1) slip plane (cross-hatched surface) of a thin FCC copper film in the bimaterial problem. Burgers vector is in the $[\bar{1}\,1\,0]$ direction: (a) 3D domain; (b) perspective of 3D domain cut along the $(\bar{1}\,1\,0)$ plane orthogonal to the (1 1 1) plane; (c) 2D screw dislocation model of the domain in (a).

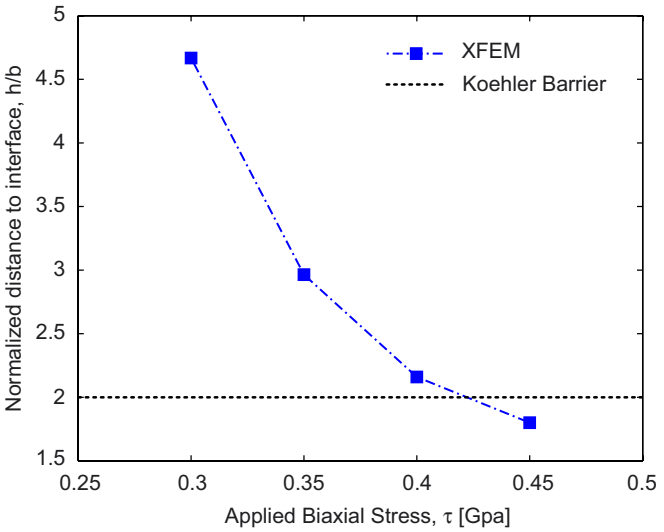

Fig. 9. Equilibrium distance of the screw dislocations from the Ni–Cu interface as a function of the applied stress.

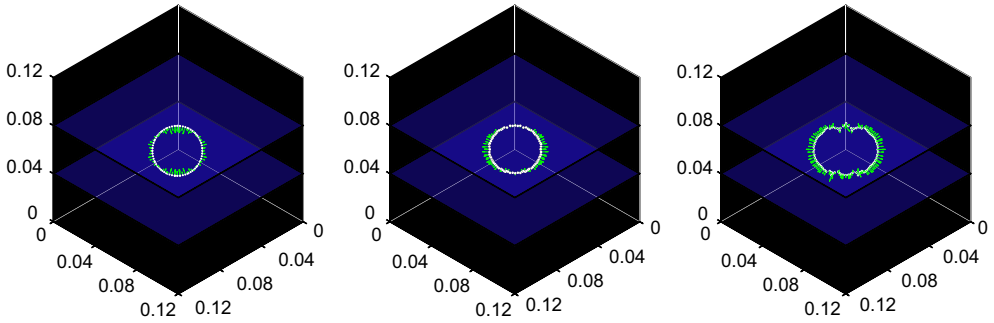

Fig. 10. Evolution of a circular dislocation loop in a layered material subjected to a shear stress: (left)—initial condition of the loop; (middle)—loop has reached equilibrium distance between top and bottom material interfaces; (right)—loop continues to expand via a threading mechanism. The blue planes indicate the interfaces between material layers and the direction of view is parallel to the (1 1 1) normal of the slip plane.

influence of any highly curved section of the dislocation line. High curvature may reduce the applied load required to cause slip across the material interfaces.

The stress predicted by XFEM is also greater than that of the threading dislocation model of Freund (1990) which predicts a critical stress of approximately 260 MPa for a Cu film with a thickness of 40 nm. This finding is consistent with the results of Ghoniem and Han (2005). Since according to our method the applied stress required for the dislocation to slip across the interface is higher, deformation in Cu films of 40 nm is therefore expected to occur by threading and not by slip across the Ni–Cu interface. This provides the motivation for a 3D model.

We next study the forces on a dislocation loop in a thin film in three dimensions using the same domain and materials as in the previous problem, see Fig. 8(a). Initially, the domain contains a single circular shaped dislocation loop on the (1 1 1) plane, in the center of the domain. The initial dislocation loop radius is 17 nm. Since the current implementation of our 3D method still utilizes the J-integral to compute the Peach–Koehler force, it is not practical to estimate the applied stress necessary to overcome the Koehler barrier because the element length would have to be on the order of a fraction of the Burgers vector. Instead, a lower stress of 75 MPa is applied, and the forces computed at the core are shown as the loop evolves in time (Figs. 10 and 11).

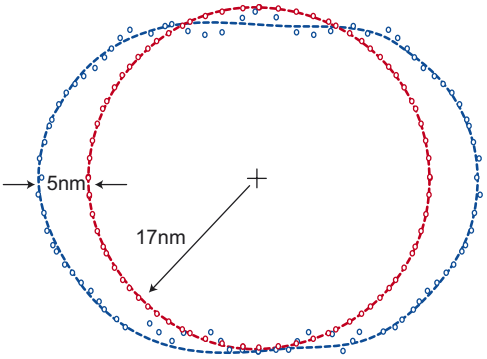

Fig. 11. Initial and evolved shapes of the dislocation loop core when subjected to a shear load of 75 MPa in a layered material (red)—initial shape; (blue)—displaced shape.

The model correctly captures the equilibrium distance between the material interfaces and the dislocation loop and shows the growth of the dislocation loop by a threading mechanism.

6. Conclusions

An improved version of a new method for modeling dislocations has been presented. The advantages of the method are that:

(1) it can be applied to nonlinear and anisotropic materials;
(2) the method is finite element based, so geometrical complexity is easily dealt with;
(3) the Peach–Koehler force is computed directly without superposition, which is of order $\mathcal{O}(n)$ complexity, as opposed to $\mathcal{O}(n^2)$ for superposition methods, where n is the number of dislocation segments;
(4) the method is simple to parallelize.

A disadvantage of the method as compared to image-field methods such as van der Giessen and Needleman (1995) is that greater resolution is required.

In the previous form of this method (Gracie et al., 2007), the discontinuity was simply terminated (with a resultant incompatibility) or terminated smoothly. In either case, the Peach–Koehler force could be evaluated quite accurately with a J-integral. However, the J-integral requires a domain of radius $3h$, and in DD applications this is a handicap. In the improved method, we have introduced enrichment functions based on the infinite domain, closed-form solution at the vicinity of the core. This enables the Peach–Koehler force to be computed directly from the finite element solution.

The applicability of the method to interface problems has been illustrated by several examples. The first example examined the convergence of the Peach–Koehler force for a bimaterial problem in two dimensions. The method is convergent both with and without core enrichment. However, the core enrichment provides a significant increase in absolute accuracy. The second example shows that the method matches the analytical expression for the stress of a dislocation loop. In the third example, the Koehler barrier was studied by determining the applied stress required to bring a screw dislocation to within two Burgers vectors of a material interface. The fourth example shows the evolution of a dislocation loop in a layered material using a discontinuous enrichment and the J-integral to calculate dislocation forces.

The singular enrichment shows many advantages over methods that only use the discontinuous enrichment, such as lower requirements in mesh refinement, and the ability to calculate the Peach–Koehler force directly. It is quite remarkable that a singular enrichment based on infinite domain solutions enables us to dramatically increase the accuracy of the method for more complex problems, such as those with interfaces. An accurate

computation of the Peach–Koehler forces needed for DD simulations then becomes possible with relatively coarse meshes. The proposed method makes possible the solution of dislocation problems which have so far been largely avoided but are nevertheless of importance.

Acknowledgments

This work was supported by the National Science Foundation, the Army Research Office and a Graduate Scholarship from the Natural Sciences and Engineering Research Council of Canada.

References

Acharya, A., 2001. A model of crystal plasticity based on the theory of continuously distributed dislocations. J. Mech. Phys. Solids 49 (4), 761–784.

Amodeo, R.J., Ghoniem, N.M., 1990. Dislocation dynamics. i. A proposed methodology for deformation micromechanics. Phys. Rev. B 41, 6958–6967.

Belytschko, T., Black, T., 1999. Elastic crack growth in finite elements with minimal remeshing. Int. J. Numer. Methods Eng. 45, 601–620.

Belytschko, T., Gracie, R., 2007. On XFEM applications to dislocations in problems with interfaces. Int. J. Plasticity. 23, 1721–1738.

Belytschko, T., Liu, W.K., Moran, B., 2000. Nonlinear Finite Elements for Continua and Structures. Wiley, New York.

Belytschko, T., Moës, N., Usui, S., Parimi, C., 2001. Arbitrary discontinuities in finite elements. Int. J. Numer. Methods Eng. 50, 993–1013.

Blanckenhagen, B., Gumbsch, P., Arzt, E., 2003. Dislocation sources and the flow stress of polycrystalline thin metal films. Philos. Mag. Lett. 83 (1), 1–8.

Bulatov, V.V., Cai, W., 2006. Computer Simulations of Dislocations, first ed. Oxford University Press, Oxford.

Cai, W., Arsenlis, A., Weinberger, C.R., Bulatov, V.V., 2006. A non-singular continuum theory of dislocations. J. Mech. Phys. Solids 54 (3), 561–587.

Chessa, J., Smolinski, P., Belytschko, T., 2002. The extended finite element method (XFEM) for solidification problems. Int. J. Numer. Methods Eng. 53, 1959–1977.

Chessa, J., Wang, H., Belytschko, T., 2003. On the construction of blending elements for local partition of unity enriched finite elements. Int. J. Numer. Methods Eng. 57, 1015–1038.

Chopp, D.L., 2001. Some improvements of the fast marching method. SIAM J. Sci Comput. 23, 230–244.

Denoual, C., 2004. Dynamic dislocation modeling by combining Peierls Nabarro and Galerkin methods. Phys. Rev. B 70 (2), 24106.

Denoual, C., 2007. Modeling dislocation by coupling Peierls–Nabarro and element-free Galerkin methods. Comput. Methods Appl. Mech. Eng. 196 (13–16), 1915–1923.

Dundurs, J., Sendeckyj, G.P., 1965. Behavior of an edge dislocation near a bimetallic interface. J. Appl. Phys. 36 (10), 3353–3354.

Eshelby, J.D., 1951. The force on an elastic singularity. Philos. Trans. R. Soc. London Ser. A, Math. Phys. Sci. 244 (244), 87–112.

Fivel, M.C., Gosling, T.J., Canova, G.R., 1996. Implementing image stresses in a 3d dislocation simulation. Modelling and Simulation Mater. Sci. Eng. 4 (6), 581–596.

Freund, L.B., 1990. A criterion for arrest of a threading dislocation in a strained epitaxial layer due to an interface misfit dislocation in its path. J. Appl. Phys. 68, 2073.

Ghoniem, N.M., Han, X., 2005. Dislocation motion in anisotropic multilayer materials. Philos. Mag. 85 (24), 2809–2830.

Gracie, R., Ventura, G., Belytschko, T., 2007. A new fast method for dislocations based on interior discontinuities. Int. J. Numer. Methods Eng. 69, 423–441.

Gravouil, A., Moes, N., Belytschko, T., 2002. Non-planar 3D crack growth by the extended finite element and level sets. Part II: level set update. Int. J. Numer. Methods Eng. 53, 2269–2586.

Groh, S., Devincre, B., Kubin, L.B., Roos, A., Feyel, F., Chaboche, J.L., 2003. Dislocations and elastic anisotropy in heteroepitaxial metallic thin films. Philos. Mag. Lett. 83 (5), 303–313.

Han, X., Ghoniem, N.M., 2005. Stress field and interaction forces of dislocations in anisotropic multilayer thin films. Philos. Mag. 85 (11), 1205–1225.

Han, C.S., Hartmaier, A., Gao, H., Huang, Y., 2006. Discrete dislocation dynamics simulations of surface induced size effects in plasticity. Mater. Sci. Eng. A 415 (1–2), 225–233.

Head, A.K., 1953. Edge dislocations in inhomogeneous media. Proc. Phys. Soc. Sec. B 66 (9), 793–801.

Hirth, J.P., Lothe, J., 1982. Theory of Dislocations, second ed., vol. 1. Wiley, New York.

Hirth, J.P., Rhee, M., Zbib, H., 1996. Modeling of deformation by a 3D simulation of multiple curved dislocations. J. Comput. Aided Mater. Des. 3 (1), 164–166.

Koehler, J.S., 1970. Attempt to design a strong solid. Phys. Rev. B 2 (2), 547–551, doi:10.1103/PhysRevB.2.547.

Kubin, L.P., Canova, G., 1992. The modelling of dislocation patterns. Scr. Metall. Mater. 27 (8), 957–962.

Lemarchand, C., Devincre, B., Kubin, L.P., 2001. Homogenization method for a discrete-continuum simulation of dislocation dynamics. J. Mech. Phys. Solids 49 (9), 1969–1982.

Moës, N., Dolbow, J., Belytschko, T., 1999. A finite element method for crack growth without remeshing. Int. J. Numer. Methods Eng. 46, 131–150.
Moran, B., Shih, C.F., 1987. A general treatment of crack tip contour integrals. Int. J. Fracture 35 (4).
Peach, M., Koehler, J.S., 1950. The forces exerted on dislocations and the stress fields produced by them. Phys. Rev. 80 (3), 436–439.
Rao, S.L., Hazzledine, P.M., 2000. Atomistic simulations of dislocation-interface interactions in the Cu–Ni System. Philos. Mag. A 80 (9), 2011–2040.
Roy, A., Acharya, A., 2005. Finite element approximation of field dislocation mechanics. J. Mech. Phys. Solids 53 (1), 143–170.
Schwarz, K.W., 1999. Simulation of dislocations on the mesoscopic scale. i. Methods and examples. J. Appl. Phys. 85 (1), 108–119.
Schwarz, K.W., Tersoff, J., 1996. Interaction of threading and misfit dislocations in a strained epitaxial layer. Appl. Phys. Lett. 69, 1220–1222.
Stolarska, M., Chopp, D.L., Moës, N., Belytschko, T., 2001. Modelling crack growth by level sets in the extended finite element method. Int. J. Numer. Methods Eng. 51 (8), 943–960.
van der Giessen, E., Needleman, A., 1995. Discrete dislocation plasticity: a simple planar model. Modelling Simulation Mater. Sci. Eng. 3, 689–735.
van der Giessen, E., Needleman, A., 2003. Dislocation plasticity effects on interfacial fracture. Interface Sci. 11 (3), 291–301.
Ventura, G., Moran, B., Belytschko, T., 2005. Dislocations by partition of unity. Int. J. Numer. Methods Eng. 62 (11), 1463–1487.
Volterra, V., 1907. Sur l'équilibre des corps lastiques multiplement connexes. Ann. Sci. Norm. Super. Sr. 3 24, 401–517.
Wang, Y.U., Jin, Y.M., Cuitino, A.M., Khachaturyan, A.G., 2001a. Nanoscale phase field microelasticity theory of dislocations: model and 3d simulations. Acta Mater. 49 (10), 1847–1857.
Wang, Y.U., Jin, Y.M., Cuitino, A.M., Khachaturyan, A.G., 2001b. Nanoscale phase field microelasticity theory of dislocations: model and 3D simulations. Acta Mater. 49 (10), 1847–1857.
Xiang, Y., Cheng, L.T., Srolovitz, D.J., Weinan, E., 2003. A level set method for dislocation dynamics. Acta Mater. 51 (18), 5499–5518.
Xiang, Y., Srolovitz, D.J., Cheng, L.T., Weinan, E., 2004. Level set simulations of dislocation-particle bypass mechanisms. Acta Mater. 52 (7), 1745–1760.